

# Force and length-dependent catastrophe activities explain interphase microtubule organization in fission yeast

**Running title:** Modelling microtubule organization in fission yeast

*Dietrich Foethke, Tatyana Makushok, Damian Brunner\* and François Nédélec\**

Cell Biology and Biophysics  
European Molecular Biology Laboratory  
Meyerhofstrasse 1, 69117 Heidelberg, Germany

Email: [nedelec@embl.de](mailto:nedelec@embl.de)  
Tel: 49-6221-387-8597  
Fax: 49-6221-387-8512

**Abstract:** The cytoskeleton is essential for the maintenance of cell morphology in eukaryotes. In fission yeast for example, polarized growth sites are organized by actin whereas microtubules (MT) acting upstream control where growth occurs (La Carbona *et al*, 2006). Growth is limited to the cell poles when MTs undergo catastrophes there and not elsewhere on the cortex (Brunner and Nurse, 2000). Here we report that the modulation of MT dynamics by forces as observed *in vitro* (Dogterom and Yurke, 1997; Janson *et al*, 2003) can quantitatively explain the localization of MT catastrophes in *S. pombe*. However, we found that it is necessary to add length-dependent catastrophe rates to make the model fully consistent with other measured traits of MTs. This result demonstrates the possibility that MTs together with associated proteins such as kinesins having a depolymerization activity can reliably mark the tips of the cell.

## Abbreviations:

MT:	Microtubule
MAP:	Microtubule associated protein
T1-T10:	Traits of the wild type cell

**Keywords:** Simulations / Cytoskeleton / Mechanics / Cell / Force

**Subject Category:** Cell Architecture

**Character Count:** ~24108 with spaces, excluding table 1

The fission yeast *Schizosaccharomyces pombe* is a convenient model to study cell morphogenesis (Hayles and Nurse, 2001). Wild type cells are simple elongated rods growing at the cell poles and dividing in the middle. Yet, previous studies have outlined an interesting interplay between shape, growth and cytoskeletal organization. The first component is the rigid cell wall surrounding yeast cells that maintains cell shape independently of the cytoskeleton. Secondly, the actin cytoskeleton is essential to cell growth and cell wall remodeling (La Carbona *et al*, 2006). Lastly, while MTs are not required for growth *per se*, they control the location of growth sites by depositing specific marker proteins (Busch and Brunner, 2004a; Busch *et al*, 2004b; Mata and Nurse, 1997; Sawin and Snaith, 2004). Abnormal deposition, occurring for example in mutants where MTs are shorter, results in cells that are either bent or branched (Sawin and Nurse, 1998; Snaith and Sawin, 2005). MTs also position the nucleus (Loiodice *et al*, 2005; Tran *et al*, 2001) and thus define the site of cytokinesis (Daga and Chang, 2005; Tolic-Norrelykke *et al*, 2005) and the partitioning of the cell into daughter cells. Hence by controlling cell growth and division, MTs impact the evolution of shape in the cell lineage. Since MTs are constrained within the cell, the converse is also true with MT organization being dependent on cell shape. For the rigid *S. pombe* cells, the two processes occur on very different time-scales; with MT lifetimes being in the order of minutes while cells typically double in size after three hours. Consequently, individual MTs are enclosed in a boundary that is effectively constant during their lifetime. This means that it is valid to first study how MTs depend on cell shape, and to later include cell shape changes. We use here computer simulation for the first step, calculating the dynamic spatial organization of MTs within a fixed cell shape. This approach complements other efforts where cell morphogenesis is modelled with reaction-diffusion equations (Csikasz-Nagy *et al*, 2008) by focussing on the MT cytoskeleton.

Interphase MTs in fission yeast are typically organized into between two and six bundles, which are usually attached to the nucleus at their middle (Tran *et al*, 2001) (Fig. 1). Antiparallel MTs overlap at their static minus-ends whereas the plus-ends are dynamic and grow from the overlap zone towards the cell poles (Janson *et al*, 2007). Such bundles transmit forces produced at the cell poles by MT polymerization to the

nucleus. In order to position the nucleus near the middle of the cell (Loiodice *et al*, 2005; Tran *et al*, 2001), MTs should efficiently target the cell poles, and have catastrophes (the switch to depolymerization) that are rare enough to enable MTs to reach the cell cortex but not so rare as to induce bending of the MT around the polar cell wall (Tran *et al*, 2001), a configuration that is not observed in wild-type cells. The most popular explanation for the timing of catastrophes involves multiple molecular activities that are assembled at the cell poles (Mata *et al*, 1997). Another possibility is that forces caused by MT polymerization feed back on MT dynamics (Dogterom *et al*, 2005). This possibility has so far not been confirmed mainly due to the lack of experimental tools *in vivo*. In this study, we have circumvented this problem using stochastic computer simulations to check if the effect of force measured *in vitro* can explain the observed MT plus end dynamics in *S. pombe*. This has involved constructing three models of MT dynamics: model F (force) in which forces at MT tips regulate MT growth and catastrophe rates, model L (length) in which MT length affects catastrophe rate, and model FL which combines both effects.

To simulate the MT cytoskeleton in *S. pombe*, we first idealized its 3D shape as a spherocylinder (see Fig. 1B and C). A nucleus and MT bundles were then added and confined within this volume. *In vivo*, MT bundles self-organize (Janson *et al*, 2007), to form overlap zones of  $0.84 \pm 0.29 \mu\text{m}$  (Tran *et al*, 2001). For the purpose of this work, it was sufficient to use fixed overlap-zones and 4 bundles, each containing 4 anti-parallel MTs, which is representative of the average situation. The nucleus was represented by a sphere, to which the overlap zones of the bundles were attached (Fig. S2). The deformations of the nuclear membrane observed *in vivo* (Daga *et al*, 2006; Tran *et al*, 2001) were incorporated into the model by attaching MT bundles to the nucleus using Hookean springs of moderate stiffness. The points to which the bundles were attached were also able to move on the nuclear surface. This allowed elongating bundles to align with the cell axis, as *in vivo* (Fig. S3). In summary, the simulation comprised bundles of flexible MTs and a connected spherical nucleus that were confined within a frictionless cortex. Whereas MT minus-ends were static, plus ends grew and shrank independently of each other thus producing polymerization forces, fiber deformation and nuclear movements. The physical equations describing the evolution of this system were solved numerically as explained before (Nedelec and

Foethke, 2007). The specific models for this study are detailed in the supplementary material.

The advantage of using *S. pombe* as a model organism is that numerous dynamical properties of MTs have been measured by light microscopy, and this enables the models to be quantitatively compared to reality. Table 1 lists the ten *in vivo* properties of MTs that were used to evaluate computational models. These ten traits summarize most of the currently established knowledge of the wild-type cells that are relevant for MT organization. Note that it was necessary to adjust the definitions of these traits to what is available from the literature (see supplementary). For example, it was important to distinguish “bundle catastrophes”, which affect the longest MT in a half-bundle from other MT catastrophes. Bundle catastrophes lead to bundle shortening, and are easy to detect experimentally. Other catastrophes are harder to observe because MTs overlap *in vivo*, and were often not reported (Brunner *et al.* ; Drummond and Cross, 2000; Tran *et al.*, 2001). Independently of the traits, characteristics of the cell geometry, MT bending elasticity and cytoplasmic viscosity were obtained from the literature or determined experimentally in the course of this study (see supplementary material). The models discussed here contain two parameters: the polymerization speed  $v_0$  ( $\mu\text{m/s}$ ) and the catastrophe rate  $c_0$  (1/s). They are evaluated by running thousands of simulations with random values of  $v_0$  and  $c_0$ , and then testing which trait was matched in each simulation. This systematic numerical exploration of the parameter space is centered on  $v_0 \sim 2.4 \mu\text{m/min}$ , which is observed under standard laboratory conditions (Tran *et al.*, 2001), and extends to regions where traits start to fail.

Model F corresponds to an *in vitro* experiment, which showed that a barrier could inhibit tubulin assembly (Dogterom *et al.*, 1997). These results were described by  $v_g = v_0 \exp(-f/f_s)$  (equation A), where  $f_s \sim 1.7 \text{ pN}$  specifies the sensitivity to force, and  $f$  is the projected force between the barrier and the MT tip (Fig. 1C). In addition, reduced assembly *in vitro* was shown to promote catastrophes according to B:  $c = 1/(a + b v_g)$  (Janson *et al.*, 2003; Janson and Dogterom, 2004). Model F used equations (A) and (B) with the forces calculated for each MT. The constants  $f_s$  and  $a$  were measured experimentally with purified tubulin. The constant  $b$  was calculated as the solution of (B) with  $c=c_0$  and  $v=v_0$  such that  $c_0$  and  $v_0$  correspond to the catastrophe

and assembly rates of unconstrained MTs. The resultant value of  $b$  differs from that measured *in vitro*, because it represents the combined effects of MT associated proteins (MAPs) present in the cell. A value for  $b$  corresponding to what was reported *in vitro* without MT regulators results in excessively long MTs that curl around the cell pole. We found that simulations with model F consistently matched T1-8 around the reference values of  $c_0$  and  $v_o$  (Fig. S1). However, these simulations fail to match T9 and T10 in this region, which lead us to investigate these traits further. Experimentally, T9 was measured in cells that are made asymmetric by centrifugation, with the nucleus ending up nearer one cell pole. It was observed that during nucleus re-centering, MTs have longer contact time with the proximal than with the distal pole ( $\sim 92 \pm 53$  s and  $\sim 46 \pm 36$  s respectively (Daga *et al*, 2006)). Model F showed opposite effects because, as shown by our simulations, MTs experience stronger compression on the proximal side than on the distal side. The other unmatched trait T10 represents the centering precision of bundles when they are not attached to the nucleus (Carazo-Salas and Nurse, 2006). To understand why T10 fails, we can consider the simpler situation of an unattached bundle made of 2 anti-parallel MTs. This bundle mechanically behaves as a single elastic beam of small viscous drag: the forces at both ends equalize very fast. Consequently, the plus tips of both MTs experience similar forces no matter where the overlap zone is located: there are little centering cues. The simulation shows that the situation with bundles of 4 MTs is essentially similar: it is centered on average, but with a large standard deviation. In conclusion, although model F matched most measurements listed in table 1, its failure to match T9 and T10 prompted us to investigate how it could be adjusted.

In the situation considered for T9, MTs are shorter on the proximal side than on the distal side, and therefore the observed asymmetry in contact times may indicate that the *length* of a MT influences its stability, which was not the case in model F. To test this possibility, we simulated a catastrophe rate that depends on MT length  $L$  according to  $c = hL / (a + bv_g)$  (equation B'). The constant  $h$  was set to  $0.2/\mu\text{m}$ , so that  $c_0$  would determine the catastrophe rate at  $L=5\mu\text{m}$  (the length at which MTs typically undergo catastrophe in average cells). This makes the resulting model FL directly comparable to model F, except that longer MTs are less stable compared to short ones. With model FL, T9 was matched with *e.g.* contact times of  $93 \pm 64$  s on the

proximal side, and  $64 \pm 39$ s on the distal side. The length-dependence overcompensated for the effects of force in a situation where the nucleus is close to the cell pole. T10 was also matched. In other words, MT bundles that are not attached to the nucleus center as observed *in vivo* (Carazo-Salas *et al*, 2006). In fact, model FL matched the 10 traits robustly with respect to  $(v_0, c_0)$  around their expected *in vivo* values (Fig. 2A). Interestingly, model FL also reproduced the shape of the distribution of MT/cortex contact times seen *in vivo* (see Fig. 3A). The precise fit shows that the experimental distribution of contact times, which is peaked around  $\sim 1$  min, is explained by the memory-less (first-order) MT catastrophe transition, because as MTs continue to grow after contact, forces building up increase the instantaneous catastrophe rate. The simulation also predicts the location of the hidden MT catastrophes (Fig. 3B), which are frequent but difficult to observe *in vivo* because these events occur on the side of a longer MT in the same bundle.

Model FL postulated length-dependent catastrophe rates to match all traits. Indeed, *Tischer et al.* have confirmed experimentally that this behavior occurs *in vivo*, observing that catastrophe rates increase linearly from  $\sim 0.1/\text{min}$  at  $L \approx 2 \mu\text{m}$  up to  $\sim 0.3/\text{min}$  at  $L \approx 5 \mu\text{m}$ , for MTs that do not contact the cell cortex (*Tischer et al. in preparation*). The measured magnitude of the dependence of catastrophe upon MT length is identical to what we have assumed, in the center of the region in which all traits are fulfilled ( $c_0 = 0.3/\text{min}$ ). It is tempting to speculate about the molecular mechanism that could mediate the destabilization of longer MTs. The *S. cerevisiae* kinesin-8 Kip3p produce a length-dependent destabilizing activity *in vitro*, because after binding at any point along the length of the MT, it moves processively to the tips, where it has a depolymerizing activity (Varga *et al*, 2006). It is possible that the two homologs of Kip3p in *S. pombe*, Klp5p and Klp6p (West *et al*, 2001) have a similar activity. Consistent with this view, the double deletion of *kfp5* and *kfp6* leads to elongated MTs that curl at cell poles (West *et al*, 2001), and reduces the length-dependence of catastrophe (*Tischer et al.*). Simulations show that length-dependent catastrophe rates offer several potential advantages to the cell. Firstly, nucleus repositioning is faster by a factor 2 in model FL compared to model F (data not shown), because proximal MTs push for a longer time than distal MTs (T9). Secondly, bundles that are observed to detach from the nucleus (Carazo-Salas *et al*, 2006; Tran *et al*,

2001) would keep their overlap regions better centered (T10), which may allow them to reattach more rapidly.

Finally, a model L having the length-dependence present in model FL, but without any force dependence also fails to fulfill all traits (Fig. S1), showing that the length-dependence is not sufficient to adjust MTs within the cell. Hence, in model FL, the established response to force together with the length-dependent MT destabilizing activity of MAPs, leads to the accurate description of the dynamics of MTs in wild type *S. pombe* cells. Remarkably, in both model F and FL, it was not necessary to assume that the cell poles had any localized activity associated to them that would affect MTs. This shows that, as anticipated (Dogterom *et al*, 2005), forces in principle are sufficient to account for the location of MT catastrophes at the cell poles.

In future work, it will be necessary to explicitly distinguish MAPs to be able to recapitulate their mutant phenotypes. To do so will require knowing how the dynamic equilibrium distribution of MAPs near MT tips is affected by force. However, having no free parameter, our current model is already predictive in calculating how cell morphology affects a *wild-type* MT cytoskeleton, and this sheds light on some mutant phenotypes. In the current model, the catastrophe rate  $c_0$  represents the combined action of all MAPs on MTs. This in particular includes the potential effect of Tea1p, Tip1p or Tea2p, which are located on growing MT plus ends. These proteins are later deposited at the cell ends, but our model does not include any influence of the deposited proteins on MTs in return. In the case of Tea1p, however, such an influence has been suggested (Brunner *et al*, 2000), because genetic deletion affects MTs. The observed defect is that MTs exhibit curling at the cell poles (see Fig. 3C). In the simulation, we noticed that cell diameter (but not cell length) affected MT curling (see Fig. 3D). This prompted us to measure MT curling *in vivo*, together with the dimensions of cells. There also, we found a clear correlation between cell diameters and the extent of MT curling (see Fig. 3E), and no correlation between cell lengths and curling. Thus the curling phenotype can be explained by the fact that *tea1Δ* cells were on average wider than wild-type cells (Fig. 3F). Furthermore, thin *tea1Δ* cells exhibited a comparable level of curling to wild type-cells of similar diameter, which confirmed that the MT phenotype is purely the consequence of the increased diameter, and that

unlike previously speculated, Tea1p has no direct influence on MT catastrophes. The variability around the average behavior is smaller in the simulation than in reality, most likely because irregularities in cell shape together with measurement errors have not been modelled. However, the average behavior was predicted correctly, since the slopes of the best linear fit between cell diameter and MT curling angles are comparable *in vivo* and in the computational model (Fig. 3D,E). In summary, it seems that *tea1Δ* cells have wild type MTs in a body that is wider than wild type. The simulation available on [www.cytosim.org](http://www.cytosim.org) can be extended to further investigate MT organization in *S. pombe*. A successful account of interphase MT dynamics, as initiated here, is a necessary step to understand the determination of cell shape in this simple organism.

The authors declare no competitive financial interests.

### **Acknowledgments:**

We thank the members of the Nedelec laboratory who contributed to cytosim. We used computers offered by IBM and maintained by EMBL/CNG and microscopes from the EMBL facility. S. Huisman, L. Murrells and I. Aprill helped with the experiments and the writing. We thank M. Dogterom, J. Gagneur, M. Kaksonen, E. Karsenti, C. Tischler and J. Ward for discussions and critically reading the manuscript. We gratefully acknowledge HFSP grant RGY84, the Volkswagenstiftung and BioMS for supporting this work.



**Table 1:** Measured features of wild type *S. pombe* cells (defined in supplementary).

<b><i>Trait</i></b>	<b><i>Description</i></b>	<b><i>Range</i></b>	<b><i>Reference(s)</i></b>
<b><i>T1</i></b>	<i>Bundle catastrophes at cells poles</i>	90–100%	(Brunner <i>et al</i> , 2000)
<b><i>T2</i></b>	<i>Bundle catastrophes in contact with the cortex</i>	90–100%	(Brunner <i>et al</i> , 2000)
<b><i>T3</i></b>	<i>Number of bundles contacting the cell poles</i>	2–6	(Daga <i>et al</i> , 2006) and this study
<b><i>T4</i></b>	<i>MT contact time with the cell pole (from contact to catastrophe)</i>	60–100s	(Brunner <i>et al</i> , 2000) and this study
<b><i>T5</i></b>	<i>Bundle length divided by cell length</i>	0.6–1.0	<i>This study</i>
<b><i>T6</i></b>	<i>Probability of seeing a curled MT</i>	0–1%	(Behrens and Nurse, 2002)
<b><i>T7</i></b>	<i>Variance of nuclear motions</i>	0–0.25 $\mu\text{m}^2$	(Daga <i>et al</i> , 2005; Daga <i>et al</i> , 2006)
<b><i>T8</i></b>	<i>Re-centering speed of initially off-centered nucleus</i>	0.2–0.9 $\mu\text{m}/\text{min}$	(Daga <i>et al</i> , 2006)
<b><i>T9</i></b>	<i>Contact times of MTs with proximal cell pole, for off-centered nucleus</i>	20–70s	(Daga <i>et al</i> , 2006)
<b><i>T10</i></b>	<i>Variance of MT bundles in enucleated cells</i>	1.4–3.4 $\mu\text{m}^2$	(Carazo-Salas <i>et al</i> , 2006)

### Figure legends

**Figure 1:** (A) *S. pombe* strain expressing GFP-tubulin and the nuclear pore marker Nup85-GFP. (B) The 3D simulation contains a spherical nucleus of radius  $1.5\ \mu\text{m}$  and MT bundles attached to it. (C) The cell of half-length  $5.5\ \mu\text{m}$  is a cylinder closed by half-spheres, of radius  $2\ \mu\text{m}$ . In each bundle, 4 MTs overlap near their minus ends, where they are linked to the nucleus. For more information, see supplementary materials.

**Figure 2: Trait success/failure diagram.** (A) To evaluate model FL, we systematically varied the growth speed  $v_0$  (x-axis) and catastrophe rate  $c_0$  (y-axis). Each symbol depicts the outcome of one simulation, summarizing its conformity with the 10 traits of table 1 (see legend). (B, C, D) Simulations circled in red in (a).

**Figure 3: Simulations compared to experiments.** (A) MT contact times with the cortex at the cell poles. Bars: Histogram of 303 measured events from 343 min of live imaging. Line: distribution predicted by model FL, for the standard parameter values (see supplementary). (B) Predicted density of catastrophes in the cell, as a function of longitudinal ( $|x|$ ) and radial ( $R = \sqrt{y^2 + z^2}$ ) positions. Top: bundle catastrophes occur mostly at the cell poles as observed. Bottom: hidden catastrophes are more distributed. (C) Fluorescence microscopy images of wild type (left) and *tea1Δ* cells (right) with GFP- $\alpha 2$  tubulin. Compared to wild type, MTs are curling more strongly in *tea1Δ* cells. (D) Simulated and (E) experimental quantification of the MT curling phenotype: the angle between the cell axis and the MT plus-end, at the time of catastrophe, is plotted as a function of cell diameter and cell length. Open symbols on the experimental plot correspond to wild-type cells, and closed symbols to *tea1Δ* cells. The best linear fit to the data is shown, and the slope of the fitted line is indicated. (F) Distribution of cell widths.

## References:

- Behrens R, Nurse P (2002) Roles of fission yeast tea1p in the localization of polarity factors and in organizing the microtubular cytoskeleton. *J Cell Biol* **157**: 783-793.
- Brunner D, Nurse P (2000) CLIP170-like tip1p spatially organizes microtubular dynamics in fission yeast. *Cell* **102**: 695-704.
- Busch KE, Brunner D (2004a) The microtubule plus end-tracking proteins mal3p and tip1p cooperate for cell-end targeting of interphase microtubules. *Curr Biol* **14**: 548-559.
- Busch KE, Hayles J, Nurse P, Brunner D (2004b) Tea2p kinesin is involved in spatial microtubule organization by transporting tip1p on microtubules. *Dev Cell* **6**: 831-843.
- Carazo-Salas RE, Nurse P (2006) Self-organization of interphase microtubule arrays in fission yeast. *Nat Cell Biol* **8**: 1102-1107.
- Csikasz-Nagy A, Gyorffy B, Alt W, Tyson JJ, Novak B (2008) Spatial controls for growth zone formation during the fission yeast cell cycle. *Yeast* **25**: 59-69.
- Daga RR, Chang F (2005) Dynamic positioning of the fission yeast cell division plane. *Proc Natl Acad Sci U S A* **102**: 8228-8232.
- Daga RR, Yonetani A, Chang F (2006) Asymmetric microtubule pushing forces in nuclear centering. *Curr Biol* **16**: 1544-1550.
- Dogterom M, Kerssemakers JW, Romet-Lemonne G, Janson ME (2005) Force generation by dynamic microtubules. *Curr Opin Cell Biol* **17**: 67-74.
- Dogterom M, Yurke B (1997) Measurement of the force-velocity relation for growing microtubules. *Science* **278**: 856-860.
- Drummond DR, Cross RA (2000) Dynamics of interphase microtubules in *Schizosaccharomyces pombe*. *Curr Biol* **10**: 766-775.
- Hayles J, Nurse P (2001) A journey into space. *Nat Rev Mol Cell Biol* **2**: 647-656.
- Janson ME, de Dood ME, Dogterom M (2003) Dynamic instability of microtubules is regulated by force. *J Cell Biol* **161**: 1029-1034.
- Janson ME, Dogterom M (2004) Scaling of microtubule force-velocity curves obtained at different tubulin concentrations. *Phys Rev Lett* **92**: 248101.

Janson ME, Loughlin R, Loiodice I, Fu C, Brunner D, Nedelec FJ, Tran PT (2007) Crosslinkers and motors organize dynamic microtubules to form stable bipolar arrays in fission yeast. *Cell* **128**: 357-368.

La Carbona S, Le Goff C, Le Goff X (2006) Fission yeast cytoskeletons and cell polarity factors: connecting at the cortex. *Biol Cell* **98**: 619-631.

Loiodice I, Staub J, Setty TG, Nguyen NP, Paoletti A, Tran PT (2005) Ase1p organizes antiparallel microtubule arrays during interphase and mitosis in fission yeast. *Mol Biol Cell* **16**: 1756-1768.

Mata J, Nurse P (1997) tea1 and the microtubular cytoskeleton are important for generating global spatial order within the fission yeast cell. *Cell* **89**: 939-949.

Nedelec F, Foethke D (2007) Collective Langevin Dynamics of Flexible Cytoskeletal Fibers. *New Journal of Physics*.

Sawin KE, Nurse P (1998) Regulation of cell polarity by microtubules in fission yeast. *J Cell Biol* **142**: 457-471.

Sawin KE, Snaith HA (2004) Role of microtubules and tea1p in establishment and maintenance of fission yeast cell polarity. *J Cell Sci* **117**: 689-700.

Snaith HA, Sawin KE (2005) Tea for three: control of fission yeast polarity. *Nat Cell Biol* **7**: 450-451.

Tolic-Norrelykke IM, Sacconi L, Stringari C, Raabe I, Pavone FS (2005) Nuclear and division-plane positioning revealed by optical micromanipulation. *Curr Biol* **15**: 1212-1216.

Tran PT, Marsh L, Doye V, Inoue S, Chang F (2001) A mechanism for nuclear positioning in fission yeast based on microtubule pushing. *J Cell Biol* **153**: 397-411.

Varga V, Helenius J, Tanaka K, Hyman AA, Tanaka TU, Howard J (2006) Yeast kinesin-8 depolymerizes microtubules in a length-dependent manner. *Nat Cell Biol* **8**: 957-962.

West RR, Malmstrom T, Troxell CL, McIntosh JR (2001) Two related kinesins, klp5+ and klp6+, foster microtubule disassembly and are required for meiosis in fission yeast. *Mol Biol Cell* **12**: 3919-3932.

Figure 1

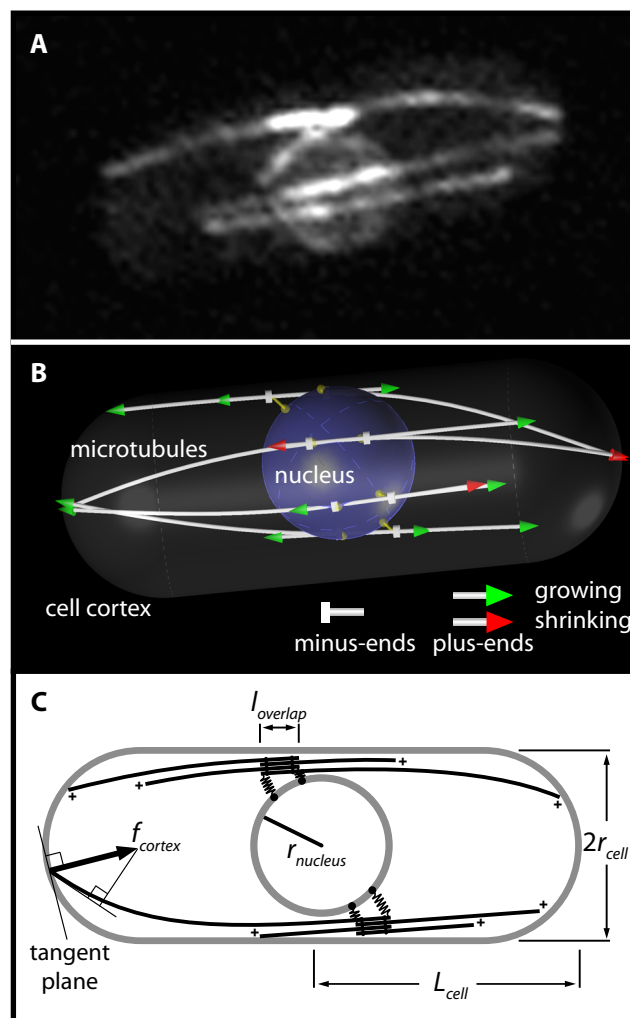


Figure 2

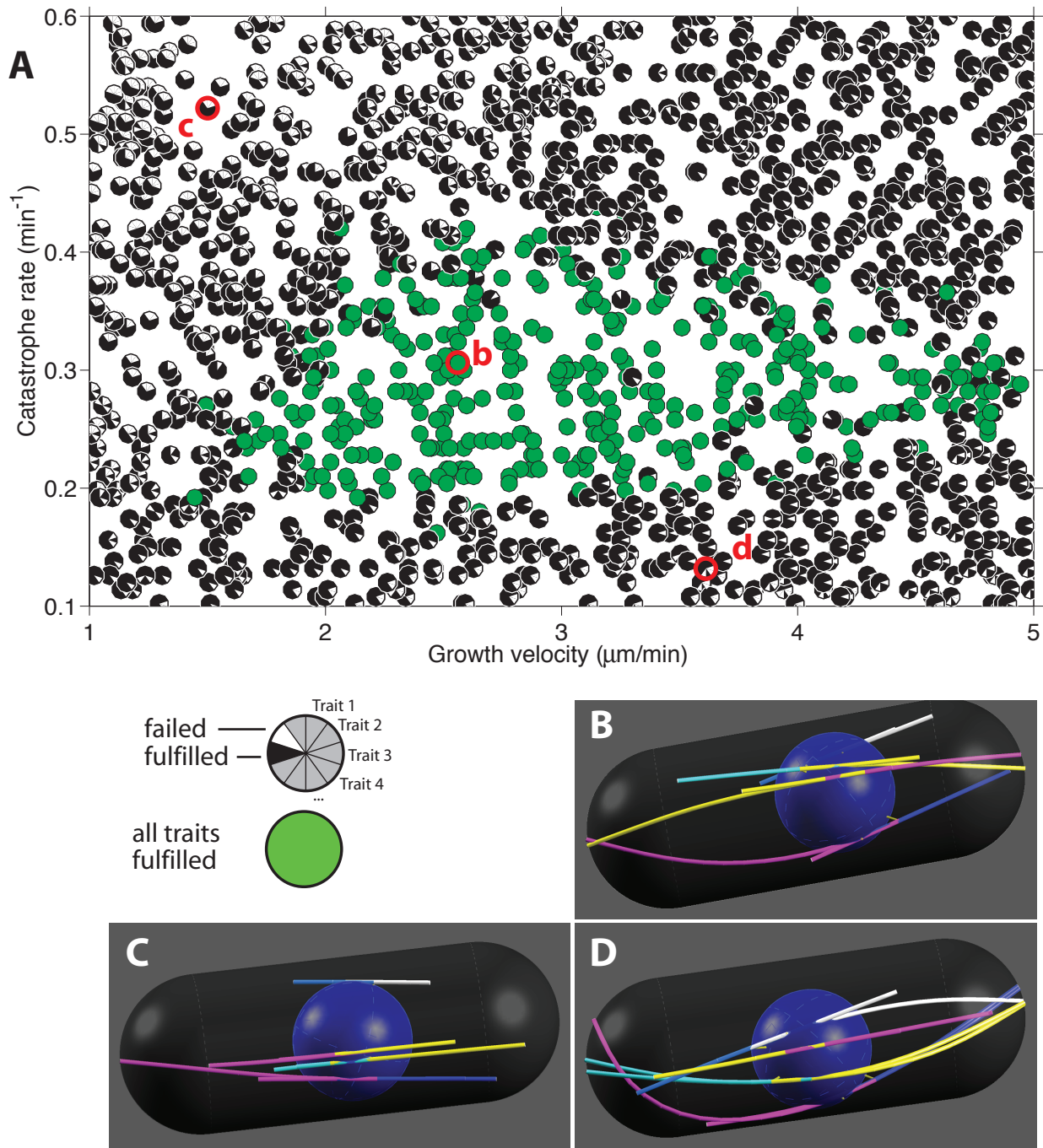
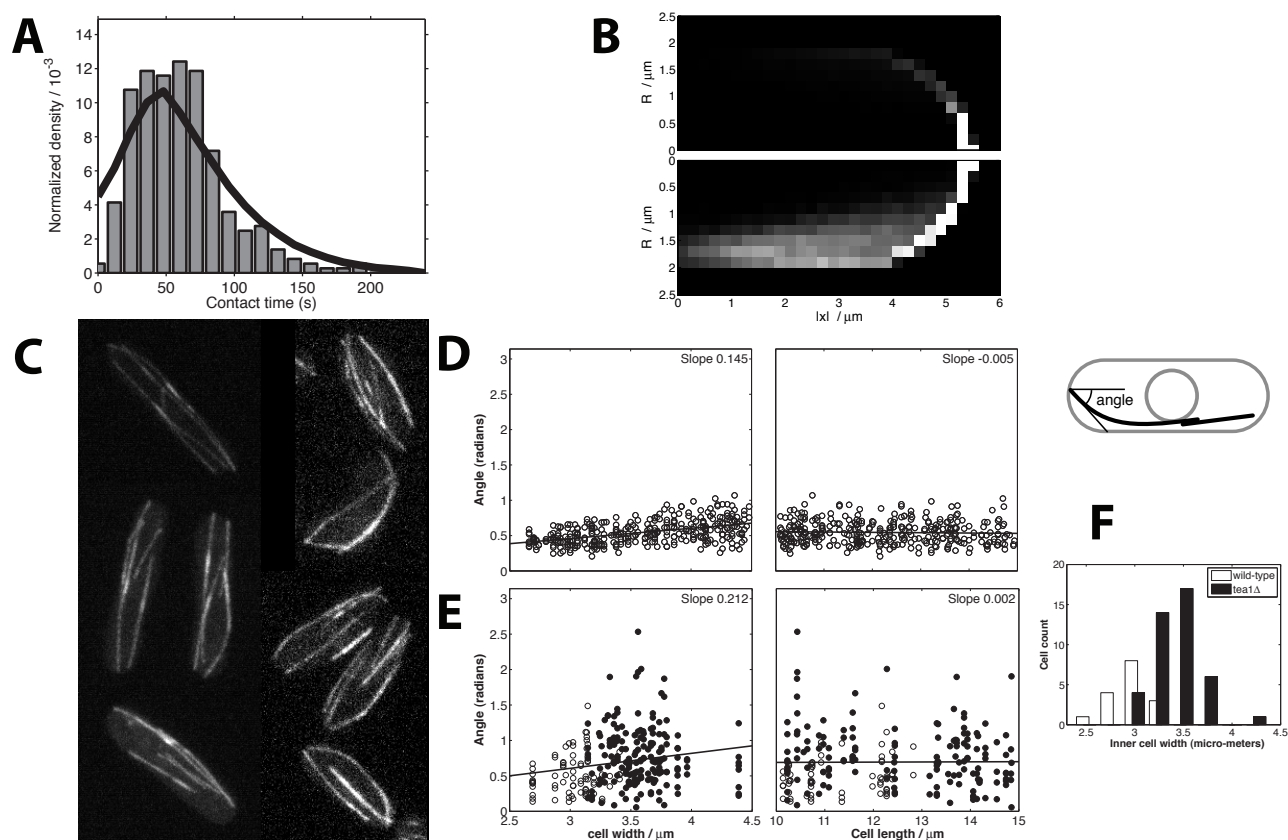


Figure 3



# Supplementary Material

Foethke et al.

## Overview

This document contains five parts (A-E): a list of supplementary movies and files; a description of the simulation methods; a detailed description of the traits listed in table 1; a description of the parameters of the simulation, with details on how their values were set from the previous literature. Finally, part E describes the methods used to generate Figure 3d and e.

## A. Online Supplementary Material

- pombeMT.dmg:** A simulation package at <http://www.microtubules.org/pombe> (currently only runs on Mac OSX, a PC version will be made available later).
- movieB.mov:** **Model FL - B** Simulation with reference parameters, exhibiting all traits of table 1.
- movieC.mov:** **Model FL - C** Simulation where MTs are too short, corresponding to Fig. 2C.
- movieD.mov:** **Model FL - D** Simulation where MTs are too long, corresponding to Fig. 2D.



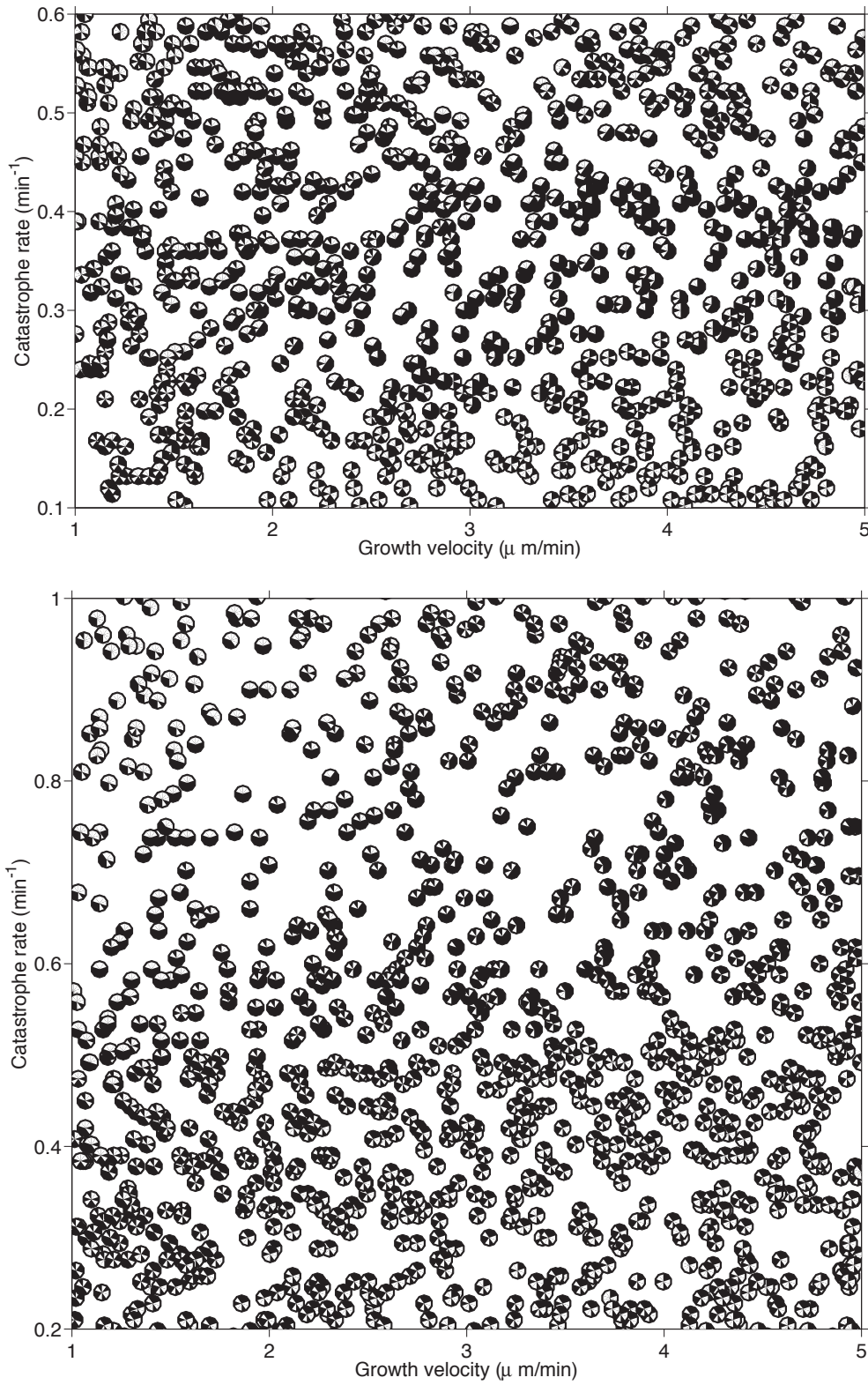


Figure S1: Summary of fulfilled traits for model F (above) that only includes the force dependence, and model L (below) that only includes the length dependence (legend are alike for main Figure 2).

## B: Simulation Methods

To analyze microtubule (MT) organization in *Schizosaccharomyces pombe* we built a computer simulation of an interphase cell. Our simulation contains MTs and a spherical nucleus. Given the physical scale of the problem, inertia can be neglected, yet Brownian motion yields a considerable contribution (1). Accordingly, over-damped Langevin equations are used to model random thermal fluctuations as well as large scale non-stochastic movements, which are set according to the laws of classical mechanics. The objects are represented by points and their mechanical properties and interactions are implemented using constraint dynamics. The simulation automatically sets and solves equations for the coordinates of the points in consecutive time steps, thus calculating the time-evolution of the system. The numerical methods used have been the subject of a detailed article (2). We present here only the components of the simulation that are specific to the current study.

The motion of an object in a viscous fluid is governed by its mobility, which relates force and speed (speed = mobility  $\times$  force). This proportionality factor can be calculated from the size and shape of the object and from the viscosity of the fluid as exemplified by Stokes's law, which describes the mobility of a sphere in an infinite fluid. For MTs, we used a variant of Stokes's law for elongated rods (3). The nucleus, however, occupies almost the whole diameter of the cell and when it moves, the counter-flow between the nucleus and the plasma membrane creates shearing forces which are stronger than in an infinite liquid. To account for this effect, we implemented a formula derived from lubrication theory (see below).

MTs and nucleus interact with the cell cortex, which is represented by a confinement potential, and also with each other. We describe the organization of MT bundles in the simulation. These bundles are attached tangentially to the nucleus at two points which are able to move on the nuclear surface. The mobility of the attachment sites is essential to allow MT bundles to orient, as observed in living cells (cf. Fig. S3). The nucleus itself is described by a rigid sphere. Yet, to mimic the deformations of the nuclear membrane observed *in vivo*, the connections between MT bundles and the nucleus are modeled as soft springs (see below). MTs within a bundle grow and shrink independently and bend according to their elastic modulus which is defined by *in vitro* measurements (see part D).

### Mobility of the Nucleus

The fluid is considered as purely viscous, and hydrodynamic interactions are ignored apart from one important effect: to move the nucleus, cytoplasm has to flow in the opposite direction, between the nucleus and the plasma membrane. The arrangement of the  $\sim 3\mu m$  nucleus inside a cell of  $\sim 4\mu m$  diameter resembles a closely fitting sphere in a cylindrical tube. The translational and rotational mobilities  $\mu^T$  and  $\mu^R$  of such a sphere were calculated for the case of an infinitely long tube (4). Assuming axial symmetry, the mobilities (expanded to lowest order in the clearance  $\varepsilon = (r_{cell} - r_{nucleus})/r_{nucleus}$ ) are:

$$\mu^T = \frac{4\varepsilon^{5/2}}{9\pi^2\sqrt{2}\eta_{cell}r_{nucleus}} \quad \mu^R = \frac{\sqrt{\varepsilon}}{2\pi^2\sqrt{2}\eta_{cell}r_{nucleus}^3} \quad (1)$$

(see Tab. 1 for an explanation of variables). For simplicity, we also used these mobilities in the transverse direction, and applied the same formulae if the nucleus was off-axis. The effect is large and results in a reduction of the translational mobility by a factor  $\sim 25$  compared to Stokes's law for a nucleus with radius  $1.5\mu m$ , or even a factor  $\sim 50$  for a radius of  $1.6\mu m$ . For comparison, an obstacle of similar size as the nucleus would yield a factor  $\sim 2$ . The mobilities are highly sensitive to the radius of the nucleus, and we therefore measured this parameter in wild type cells (see part D).

## Confinement

In the simulation, the cortex is immobile and undeformable. To represent an idealized wild type *S. pombe* cell, we used a spherocylinder, *i.e.* a cylinder of length  $2l_{cylinder}$  and radius  $r_{cell}$  closed by two half-spheres (cf. Fig. 1B). Any model-point  $\mathbf{x}$  inside this volume is free of confinement force. A point outside is subject to a force  $\mathbf{f}(\mathbf{x}) = k_{cortex}(\mathbf{p}(\mathbf{x}) - \mathbf{x})$ , where  $\mathbf{p}(\mathbf{x})$  is the point on the cortex with the shortest distance to  $\mathbf{x}$ , *i.e.* the orthogonal projection of  $\mathbf{x}$  on the cortex. By definition the force is always directed towards the inside of the cell, and perpendicular to the cortex. It thus represents a boundary with no friction, which is the case in *S. pombe* during interphase.

## Microtubule Bundles

For simplicity, the structure of MT bundles in the simulation is static and the bundles are constructed as shown in figure S2. Four MTs are crosslinked together by Hookean springs of stiffness  $k_{bundle}$ . Each connection creates an attractive force between the minus end  $\mathbf{m}_i^-$  of the  $i$ -th MT and a point  $\mathbf{x}_j$  at distance  $l_{overlap}$  from the minus end of the  $j$ -th MT. To satisfy the action-reaction principle,  $\mathbf{f} = k_{bundle}(\mathbf{x}_j - \mathbf{m}_i^-)$  is applied to  $\mathbf{m}_i^-$ , while  $-\mathbf{f}$  is applied to  $\mathbf{x}_j$ .

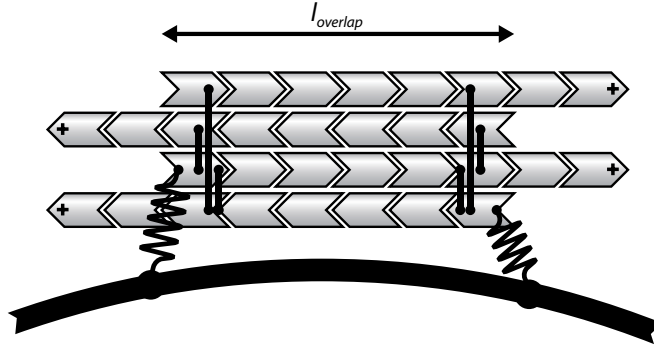


Figure S2: **Construction of microtubule bundles and their connection to the nucleus.**

Each bundle in the simulation consists of MTs connected as shown here by the straight vertical lines. MTs within the bundle alternate in direction so as to create a balanced overlap of size  $l_{overlap}(1.0\mu m)$ . Furthermore, each bundle is attached to the nucleus at the edges of the overlap zone with two softer elastic links, shown as springs. The fibers in the simulation have no width, and the Hookean links of zero resting length make them overlap, unlike in this sketch.

Six connections in the bundle generate an antiparallel overlap of length  $l_{overlap}$ . The exact arrangement of the links does not affect the simulation outcome, since  $k_{bundle}$  is high relative to MT polymerization forces (data not shown). The unconnected parts outside the overlap zone may bend away from each other. This happens when one of the MT contact the cortex, as observed *in vivo*.

## Attachment of Microtubule Bundles to the Nucleus

In interphase, MT bundles are mechanically linked to the nucleus (5). Because of these links, MTs are able to reposition the nucleus when they grow and push against the cell cortex. In the simulation, each bundle is attached to the sphere at two points, which are linked to the minus ends of two MTs of the bundle (cf. Fig. S2). The link between a MT minus end  $\mathbf{m}^-$  and its corresponding surface-point

$\mathbf{n}$  on the nucleus has a stiffness  $k_{link}$ . The action-reaction principle is satisfied by applying the force  $\mathbf{f} = k_{link}(\mathbf{n} - \mathbf{m}^-)$  to  $\mathbf{m}^-$ , and the opposite force to  $\mathbf{n}$ .

The stiffness  $k_{link}$  is chosen to mimic the elasticity of the nuclear membrane. Since the points on the nucleus behave like buoys in a fluid, MT bundles are coupled only indirectly. Strong couplings arise only when a bundle moves the entire nucleus, and not only the surface-points to which it is attached. In general, the motions of a surface point have little influence on the other points (and bundles), as long as they are small compared to the radius of the nucleus. As expected, however, moving a surface-point by more than  $r_{nucleus}$  hauls the entire nucleus including all MT bundles.

## Dynamic Instability of Microtubules

In the simulation the dynamics of individual MTs are not correlated within a bundle, i.e. all MTs grow and shrink independently. MT minus ends are static and stay attached to the nucleus while the plus ends are either growing or shrinking. Catastrophes occur with a rate  $c$  which is either a function of force (model F) or a function of force and MT length (model FL). According to experimental observations (6) shrinking MTs never rescue in the cytoplasm. For simplicity, we assumed that MTs regrow immediately if they shrink into the overlap region. This leaves three parameters common to all models: the growth velocity  $v_g$ , shrinkage speed  $v_s$  and catastrophe rate  $c$ . The shrinkage velocity  $v_s$  is constant in all models used in this study. They were defined as follows:

### 1. Model F: Force dependent microtubule dynamics

Growth velocity and catastrophe rate depend on the force experienced by MT plus ends. We implemented the *in vitro* finding (7) that the assembly rate of tubulin at MT tips is slowed down by an opposing force  $f$ :

$$v_g(f) = v_0 e^{f/f_s} \quad (f \leq 0) \quad (2)$$

Here,  $v_0$  is the maximum growth velocity obtained for MTs that do not touch the cortex and are not under compression. The parameter  $f_s$  can be interpreted as the sensitivity of MT growth to the opposing force. The scalar  $f$  used in equation (2) is calculated from the projection of the force vector  $\mathbf{f}$  (acting on the MT plus end) on the direction of MT growth. If  $\mathbf{e}^+$  denotes the unit vector pointing in the direction of growth at the MT plus end, we use  $f = \mathbf{f} \cdot \mathbf{e}^+$ . In the simulation, forces originating from interactions with the cortex are always compressive (see Fig. 1C), and the growth speed can only be reduced ( $f \leq 0$ ).

In addition to slowing-down MT polymerization, the force increases the probability of a MT to undergo catastrophe. *In vitro* experiments with pure tubulin indicated that a linear relationship exists between the catastrophe time  $t_{cat} = 1/c$  and the growth speed  $v_g$  of MT plus ends (8):

$$c = (a + b v_g)^{-1} \quad (3)$$

We can relate the two constants  $a$  and  $b$  to the ‘minimum’ catastrophe rate  $c_0$  obtained for MTs growing under zero force ( $v_g = v_0$ ), and to the ‘maximum’ catastrophe rate  $c_{stalled}$  reached for stalled MTs ( $v_g = 0$ ):

$$\begin{aligned} 1/c_{stalled} &= a \\ 1/c_0 &= a + b v_0 \end{aligned} \quad (4)$$

We varied  $c_0$ ,  $v_0$  systematically in our study, and  $a$  and  $b$  are calculated using equations (4). The growth and catastrophe rates of each MT are then calculated using equations (2) and (3). Model

F thus introduced two additional parameters: the sensitivity to force  $f_s$  and the catastrophe rate at speed zero  $c_{stalled}$ . Both values are set exactly to what has been observed *in vitro* (7, 8):  $f_s = 1.67 \text{ pN}$ , and  $1/c_{stalled} = 24 \text{ s}$  (see part D: Parameters of the Simulation).

## 2. Model L: Length- dependent microtubule dynamics

The model does not include the effect of force. The growth speed  $v_0$  is constant, and catastrophe rates are length-dependent:

$$c = hLc_0, \quad (5)$$

where  $L$  is the current length of the MT. Note that changing the value of  $h$  shifts the diagram in figure 2 along the  $c_0$ -axis, but does not alter the results otherwise. This is because in reality, only the combined value  $hc_0$  is used in the simulation. We thus fixed  $h = 0.2 \mu\text{m}^{-1}$  such that  $c_0$  represents the catastrophe rate for a MT of length  $5 \mu\text{m}$ , which is the typical length of MTs in our simulated cells of length  $11 \mu\text{m}$ . In this way, the diagram for model L is minimally shifted, and thus directly comparable to the diagram obtained for model F.

## 3. Model FL: Force and length- dependent microtubule dynamics

The model is similar to model F, except that equation (3) is replaced by:

$$c = hL/(a + bv_g), \quad (6)$$

where  $L$  is the current length of the MT. As before, we fixed  $h = 0.2 \mu\text{m}^{-1}$ . The values of  $a$  and  $b$  are calculated from the parameters of the simulation as for model F.

**Implementation:** MTs in the simulation grow and shrink continuously at a speed of  $v_g$  or  $v_s$  respectively. Equation (2) is compatible with a thermal-ratchet mechanism, but we did not model tubulin assembly stochastically. Instead, growing MTs are elongated by  $v_g\tau$  at their plus end in each time interval  $\tau$ . The time step  $\tau$  (0.01s) is chosen such that at a growth speed of  $0.04 \mu\text{m}/\text{s}$ , the elongation ( $0.5 \text{ nm}$ ) is small. Catastrophe events however, are rare and were therefore modeled stochastically: To decide if a catastrophe occurred during the time interval  $\tau$ , the cumulative probability  $P(c, \tau) = 1 - e^{-c\tau}$  is compared to a pseudo-random number  $\theta$ , which is uniformly distributed in  $[0, 1]$ . The dynamic state of the MT is changed, if  $\theta < P(c, \tau)$ . This choice is made independently for all MTs and is repeated at each time step  $\tau$  (which is such that  $c\tau \ll 1$ ).

## C: The 10 Traits

Characteristics of interphase MTs in wild type *S.pombe* (cf. Table 1) were used to quantitatively evaluate the simulations. In the following paragraphs the traits are discussed together with their methods of quantification. The experimental quantifications were either performed by ourselves or values were taken from the literature. The simulated quantifications were adjusted to match the experimental methods, to enable direct comparisons. For T1 to 7, the simulation was started with the nucleus in the center of the cell. For T8 and T9, the nucleus was initially near the cell pole (its center at  $x = 3.5\mu m$ ). For T10, the nucleus was absent from the simulation.

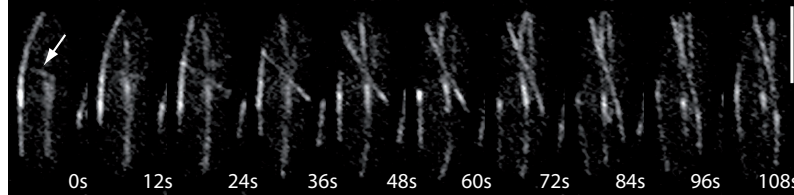


Figure S3: Time series of a wild type cell expressing GFP-tubulin. A MT bundle, newly nucleated on the nucleus (arrow) aligns parallel to the long cell axis. The new bundle rotates relative to the existing ones, indicating that interphase MT organizing centers (iMTOCs) are mobile on the nuclear surface. The images shown are maximum projections of single planes taken on a spinning disc confocal microscope with a z-spacing of  $0.5\mu m$ . scale bar:  $5\mu m$

Our simulation was also built to be able to match one important feature of *S. pombe*: short MT bundles nucleated in random directions orient themselves as they elongate (Fig. S3 and supplementary movie S1). Since the new bundle rotates relative to the existing ones during this period, it is thought that the bundle attachment sites are mobile on the nuclear surface. In this way, MT bundles can align parallel to the long cell axis. In the simulation this important feature is granted by the ‘fluidity’ of the nuclear envelope (see part B). This feature was not used in the evaluation, since it was always fulfilled under reasonable parameter values.

### T1: Catastrophes at Cell Poles

Previous measurements revealed that more than 90% of all ‘catastrophes’ in wild type cells occur at the cell poles (9). However, in this and similar studies, single MTs within a bundle could not be resolved efficiently and their dynamic behavior could not be quantified. Hence only catastrophes of the longest MTs within each half-bundle were recorded. Catastrophes of shorter MTs were not detected. In order to be able to compare the simulation to the published data, only bundle catastrophes were registered. T1 was considered to be fulfilled, if more than 90% of all bundle catastrophes occurred in the cell caps.

### T2: Catastrophes at the Cortex

In wild type cells more than 95% of all bundle catastrophes were reported to occur at the cortex (9).

However, due to the limited resolution of optical microscopy, all catastrophes happening within a distance of  $\sim 0.5\mu m$  from the cell edge were probably scored as cortical. To compare with the *in vivo* measurements, bundle catastrophes in the simulation were therefore also registered, if they happened closer than  $0.5\mu m$  to the edge of the cell. T2 was fulfilled if the fraction of cortical bundle catastrophes represented 90% or more of all bundle catastrophes.

### T3: Number of Half-Bundles Touching the Poles

The number of half-bundles touching the poles at any time was recently published to be  $1.5 \pm 0.4$  (5). However, it was not specified exactly how bundles were scored and how many bundles the measured cells contained. We therefore repeated the measurement, counting 498 half-bundles in 73 cells (Fig. 4) in wild type cells expressing GFP- $\alpha$ 2tub from a single ectopically integrated gene copy (10). A half-bundle was considered to be touching the cell pole if it was in contact with the cortex within the curved region of the cell.  $3.6 \pm 1.2$  half-bundles touched the poles, out of a total of 6.8 half-bundles per cell on average.

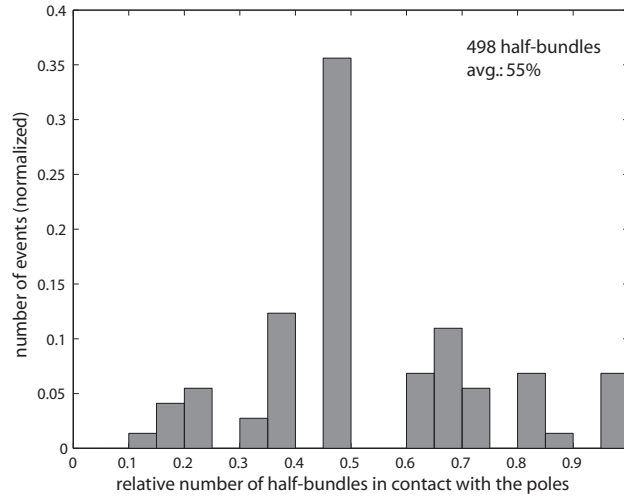


Figure S4: **Fraction of half-bundles touching the cell poles.**

Thus about  $55 \pm 21\%$  of all half-bundles touch the cell poles at any time. Since the simulation contains eight half-bundles, and to account for the stochastic variations during the simulation, we regarded T3 to be fulfilled, if the number of touching half-bundles was between 2 and 6.

### T4: Microtubule Contact Time at Cell Poles

MTs in contact with the cell poles grow with a reduced polymerization rate (6, 11), which allows them to stay in contact with the cortex up to 200s without curling (6, 9). For both, experiment and simulation, contact was defined from the moment a MT touched the cortex within the cell cap, to the frame at which depolymerization was detected. Previous measurements of the average contact time yielded different values: 75s (9), 90s (6) and 83.7s (5). T4 was therefore considered to be fulfilled if the average contact time in the simulation was between 60 and 100s.

To measure the distribution of contact times with higher precision *in vivo* than previously, we acquired time-lapse movies of wild type cells expressing GFP- $\alpha$ 2tub (as in T3) at 3 frame/s and analyzed them visually using custom written macros in ImageJ. Our measurements are consistent with the previously published results. However, we obtained the *distribution* of contact times, which provided a potent test of the model (see Fig. 3A).

### T5: Microtubule Bundle Length

Recently, high-resolution data on individual MT was obtained by electron tomography (12). However, the number of MTs measured in this way is relatively low. Using optical microscopy on cells expressing GFP- $\alpha 2$ tub (as in T3), individual MT could not be detected, but we could easily determine the length of entire MT bundles. We found that MT bundles covered 70% of the cell length on average (Fig. 5), as determined from maximum intensity projections (133 bundles were scored in 36 cells).

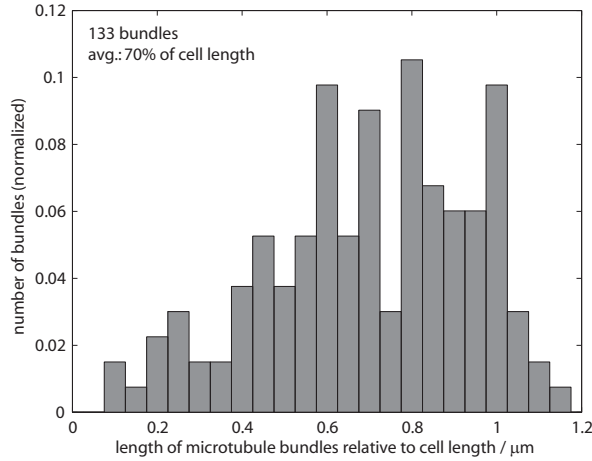


Figure S5: **Relative total MT bundle length *in vivo*.**

To compare the output from the simulation to the *in vivo* measurement the full bundle length was also projected in the z-direction (the difference between the z-projected and the full length was below 3%, since bundles are usually aligned). T5 was considered to be fulfilled, if the bundle length was above 60% of the cell length.

### T6: Microtubule Curling

MTs in wild type cells often bend when they push against the cortex. Yet they almost never curl around the cell poles such that the MT plus ends point towards the nucleus. The amount of curling MTs in wild type cells is below 1% (13). In the simulation, we quantified the amount of curling by considering every MT during the course of a simulation. Mathematically, the test was based on the tangential vectors at the minus end ( $\mathbf{m}$ ) and at the plus end ( $\mathbf{p}$ ), which point in the same direction when the MT is straight. A MT was considered curling if the scalar product  $\mathbf{m} \cdot \mathbf{p}$  was negative, meaning that the MT ends make an angle of 90 degrees or more. T6 was considered to be fulfilled, if the fraction of curling MTs was less than 1%.

### T7: Variation of Nuclear Position

The equilibrium position of the nucleus at the cell center is reached before cytokinesis and is maintained until the cell progresses into mitosis. Yet, throughout interphase MTs constantly pull on the nuclear envelope while they are pushing at the cell ends, and the nucleus continuously moves around the cell center by approximately  $\pm 0.2 \mu\text{m}$  (14). We considered T7 to be fulfilled, if the variance was lower than  $0.25 \mu\text{m}^2$ .



## T8: Active Centering of the Nucleus

Several observations have indicated that, *in vivo*, the nucleus is centered by MT bundles pushing on the cortex (5,6). Cells treated with MT depolymerizing drugs like methyl-2-benzimidazole-carbamate (MBC) or thiabendazole (TBZ) do not exhibit active displacements of the nucleus, confirming this mechanism (6). Interestingly, the nucleus is moved off-center, and repositioned at every cell cycle. During anaphase the two daughter nuclei are pushed into the cell poles by the elongating spindle. After spindle breakdown the nuclei are repositioned to the center by cytoplasmic MT bundles. As interphase resumes the center position is maintained, even if the cells grow only at one pole before ‘new end take off’ (NETO).

In cells in which the nucleus was artificially misplaced by centrifugation, it moved back to the cell center with a maximum speed ranging from 0.24 to 0.82  $\mu\text{m}/\text{min}$  (5). To test if MTs could reposition the nucleus with a similar speed in the simulation, the center of the nucleus,  $n_0$ , was initially positioned at the edge of the central cylinder (at  $x = 3.5\mu\text{m}$ ). The centering speed of the nucleus was obtained by fitting a line to the nucleus positions within the first 50 – 200s of the simulation. To match the *in vivo* measurements, T8 was considered to be fulfilled if the speed of the nucleus was between 0.2 and 0.9  $\mu\text{m}/\text{min}$ .

## T9: MT Contact Times with off-centered Nucleus

In cells in which the nucleus was artificially misplaced by centrifugation, MTs on the side of the nucleus close to the cell pole (the proximal side) were shown to have longer contact times (92s) than the MTs facing the other pole (46s at the distal side, (5), table 1).

In the simulation, we tested this behavior by fixing the nucleus near the cell pole (at  $x = 3.5\mu\text{m}$ ) and analyzed the MT contact times at the proximal and distal poles. This gives numbers which are similar to the case where the nucleus is able to move, because the nucleus moves slowly (data not shown), but enables more events to be recorded. T9 was fulfilled if the average contact time at the proximal pole was between 20 and 70s longer than at the distal pole.

## T10: Centering of MT Bundles

MTs are able to form bundles that align with the long cell axis even in the absence of the nucleus (15). To determine the position of the bundle overlap region in such enucleated cells, the antiparallel bundling protein Ase1 was labeled with GFP and imaged using fluorescence microscopy. It was shown that the position of the overlap is normally distributed around the cell center with a variance of  $\sigma^2 \approx 2.37\mu\text{m}^2$  (we deduce  $\sigma$  from the report that 75% of the total signal is within 1.77  $\mu\text{m}$  for enucleated cells (15), which thus corresponds to  $1.15\sigma$  for a normal distribution).

To compare the centering of MT bundles in enucleated cells to our model, simulations were run without the nucleus. The position of the 1  $\mu\text{m}$  overlap was summed over all bundles and time frames in analogy to the evaluation of the fluorescence data. T10 was fulfilled if the variance of the overlap position was between 1.4 and 3.4  $\mu\text{m}^2$ .

**Note:** We could simulate a cell with 3 attached bundles and one free one, to match the recent observation that bundles are not always attached to the nucleus (15). However, the properties of such a cell can already be mostly deducted from the results of a simulation with attached bundles, and from a simulation with only unattached bundles. It is unlikely to provide additional insights.

## D: Parameters of the Simulation

The input parameters of the simulation are of three sorts:

1. The MT growth speed and catastrophe rate. We decided to vary these parameters because they have a great influence on the system.
2. The second group contains parameters that have been measured experimentally, and that were taken as constants in our study. Values for these parameters were determined experimentally, either in wild type cells or *in vitro*. We adopted the values measured by other groups without modifying them.
3. The last group are numerical parameters associated to the methods used to solve the system, e.g. the integration time step  $\tau$ , or associated with our simplification of the physical reality (for example, having only a few links between the MTs to make the bundles). The results of the simulations are essentially independent of these values, beyond a precision threshold (for example, the time-step needs to be small enough).

All parameters are listed in table S1, with their values corresponding to a wild type cell under standard laboratory conditions. In model FL, simulations run with this reference set fulfilled all traits consistently. To probe the system, parameters were varied one by one while keeping the others at their reference value (see Dietrich Foethke’s PhD thesis). We describe below how the values were set, citing the relevant sources. They can be changed in the simulation package available on <http://www.cytosim.org>.

### Cell Size

Two parameters characterize a spherocylinder: the half-length  $l_{cylinder}$  of the cylinder and the cell radius  $r_{cell}$ . Since the cylinder is closed by half-spheres, the cap radius is equal to the cylinder radius and the resulting total cell length is  $l_{cell} = 2(l_{cylinder} + r_{cell})$ . Wild type *S. Pombe* grow from 7 to 14  $\mu m$  in length (6) while maintaining a constant diameter of  $\sim 4 \mu m$ . We therefore used  $r_{cell} = 2 \mu m$  and  $l_{cylinder} = 3.5 \mu m$  to simulate a cell with an average length of 11  $\mu m$ .

### Stiffness of the Cortex

At the level of light microscopy MT pushing forces do not deform the cortex, which is covered by a rigid cell wall. Below this scale the elastic properties of the cortex and its response to force are unknown. For simplicity, in the simulation the cortex is represented by a harmonic potential. The elastic modulus  $k_{cortex}$  directly relates MT polymerization forces to the distance by which a MT can indent the cortex from its equilibrium position. We used a stiffness of  $k_{cortex} = 200 pN \mu m^{-1}$ , leading to protrusions of  $\sim 25 nm$  at a typical MT polymerization force of  $\sim 5 pN$ . Protrusions that small correctly represent the steadiness of the cell wall observed *in vivo* by light microscopy, but any higher values would work equally well (data not shown).

### Viscosity of the Cytoplasm

The viscoelastic properties of the *S. pombe* cytoplasm were investigated by observing the motion of lipid granules of radius 150 nm in living yeast cells (16). It was shown that the granules exhibit subdiffusive behavior at time scales between  $10^{-4}$  and  $10^2 s$  which is thought to be caused by the presence of polymer networks and membranous structures. Above 1 s however, some granules diffused normally

## Parameters (varied in Fig. 2)

### Microtubules

free growth velocity	$v_0$	$0.04 \mu\text{m}/\text{s}$
free catastrophe rate	$c_0$	$0.005 / \text{s}$

## Constants

### Cortex and Cytoplasm

cell radius	$r_{\text{cell}}$	$2 \mu\text{m}$	
half-length of cell body	$l_{\text{cylinder}}$	$3.5 \mu\text{m}$	(total cell length is $11 \mu\text{m}$ )
effective viscosity of the cytoplasm	$\eta_{\text{cell}}$	$0.9 \text{ pN s} / \mu\text{m}^2$	

### Nucleus

radius	$r_{\text{nucleus}}$	$1.5 \mu\text{m}$
mobility of anchoring buoys	$\mu^S$	$0.05 \mu\text{m} / \text{pN s}$
membrane elasticity	$k_{\text{nucleus}}$	$20 \text{ pN} / \mu\text{m}$

### Microtubules

flexural rigidity of MTs	$\kappa_{\text{mt}}$	$30 \text{ pN} \mu\text{m}^2$	
shrinkage velocity	$v_s$	$0.15 \mu\text{m}/\text{s}$	(negative in the configuration file)
sensitivity to force	$f_s$	$1.67 \text{ pN}$	
catastrophe rate for stalled MT	$c_{\text{stalled}}$	$0.04 / \text{s}$	(catastrophe time of $25 \text{ s}$ )

### Microtubule Bundles

number of bundles	$N_{\text{bundle}}$	4
number of MTs per bundle	$N_{\text{mt}}$	4
width of the overlap region	$l_{\text{overlap}}$	$1 \mu\text{m}$

## Numerical

stiffness used for confinement	$k_{\text{cortex}}$	$200 \text{ pN} / \mu\text{m}$
stiffness used to bundle MTs	$k_{\text{bundle}}$	$1000 \text{ pN} / \mu\text{m}$
time step	$\tau$	$10 \text{ ms}$
convergence threshold	$\psi$	0.1
MT segmentation length	$\rho$	$0.5 \mu\text{m}$

Table S1: Parameters of the simulation, symbols and reference values. The constants are set according to measurements in wild type cells or *in vitro*, as described in the text. “Numerical” parameters are chosen to numerically solve the model with sufficient precision.

(cf. Fig.3 in (16)). At this time scale, we used Stokes's law together with the Einstein-Smoluchowski relation, to estimate the effective viscosity of the cytoplasm. Since the particles are small compared to the radius of the cell the effects of lubrication flow were neglected in this calculation. From Fig. 3 in (16) we determined a mean square displacement of  $\langle \Delta r^2 \rangle = 10^{-2} \mu m^2$  at a time lag of 1s, which results in an effective viscosity of  $\eta \approx 0.9 pNs/\mu m^2$ , i.e.  $900\times$  water. For simplicity, we assumed a purely viscous behavior of the cytoplasm in our simulations and used this value.

## Radius of the Nucleus

Because of the counter-flow between the nucleus and the cortex the mobility of the nucleus is highly sensitive to the size of the gap  $r_{cell} - r_{nucleus}$ . Changing  $r_{nucleus}$  from  $1.5\mu m$  to  $1.6\mu m$  reduces the predicted mobility by a factor 2 (see B: Simulation Methods). This prompted us to determine the relative size of the gap *in vivo*, using wild type cells transformed with pD817, a plasmid encoding for GFP-cytochrome P450 reductase to label nuclear and plasma membranes.

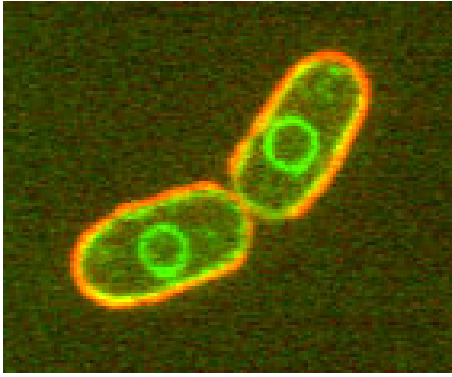


Figure S6: Measuring the size of the cell and the nucleus. The image shows a maximum projection of the central slices from a z-stack ( $\Delta z = 0.5\mu m$ ). The plasma membrane and the nucleus are shown in green, the cortex in red.

Additionally, cells were incubated with TRITC-lectin to label the cell cortex from the outside (Fig. S6). Images were taken with a spinning disc confocal microscope. The radius of the nucleus was determined from maximum projections by fitting a circle to the GFP-signal. A circular Hough transformation was used to automatically detect the nuclei and measure their radii. To determine the size of the cell the plasma membrane and the cortex were fitted to the shape of an idealized pombe cell, i.e. a rectangle closed by two half-circles. A Gauss-Newton method was implemented to minimize the geometric distance to the cell outline. The average of the two short half-axis was then used for the cell radius. The fitting was done semi-automatically with custom macros in Matlab. We found  $r_{nucleus}/r_{cell} \approx 0.75$ , i.e.  $r_{nucleus} = 1.5\mu m$  for  $r_{cell} = 2\mu m$  ( $n = 56$  cells). For a more extensive characterization, see (17).

## Mobility of “Buoys” in the Nuclear Membrane

Little is known about the identity of the molecules involved in anchoring MT bundles to the nucleus. Possible candidates are Mia1p (18) and Mto2p (14). To estimate the mobility of the anchoring points in the simulation, we therefore considered the Spindle Pole Body (SPB) which is the most prominent of the MT anchors *in vivo*. In interphase the SPB is embedded in the nuclear membrane, generating one MT bundle. In electron microscopy it is observed as an oblate ellipsoid with a thickness of  $h = 90nm$  and a radius of  $r = 90nm$  (19). These dimensions can be used to calculate its mobility in the membrane using the Saffman-Dellbrück equation (20) which describes the mobility of a cylindrical object in a thin membrane surrounded by a viscous fluid:

$$\mu^s = \frac{1}{4\pi\eta_{nucleus}h} \left( \ln \frac{\eta_{nucleus}h}{\eta_{cell}r} - \gamma \right) \quad (7)$$

where  $\gamma$  is Euler's constant and  $\eta_{nucleus}$  is the viscosity of the nuclear membrane. Assuming that  $\eta_{nucleus} \sim 10 \cdot \eta_{cell}$ , we find  $\mu^s \sim 0.17\mu m/pNs$ . In wild type cells the mobility of the SPB is most

likely further limited by the chromosomes being attached to the nucleoplasmic face of the SPB. Therefore we used  $\mu^S = 0.05\mu\text{m}/pNs$  in our simulations.

## Microtubule-Nucleus Steric Interaction

The simulation includes a repulsive interaction between the nucleus and any part of a MT inside the sphere of radius  $r_{nuc}$  around the center of the nucleus. This interaction is mediated by the elastic nuclear membrane *in vivo* of stiffness  $k_{nucleus}$ . The repulsion is implemented independently of the links between the nucleus and MT bundles. Its removal did not change the results (Figure 2 is almost identical, data not shown).

## Stiffness of Microtubule-Nucleus Links

*In vivo* the nucleus visibly deforms under forces transmitted by the attached MT bundles (5, 6, 14). For this reason the motion of the nucleus and its bundles is thought to be only coupled 'softly'. Forces transmitted on the nucleus are attenuated, but nevertheless determine its motion at long time scales. Extreme deformations can reach  $\sim 1\mu\text{m}$  (5) and are driven by MT polymerization, which produces forces in the range of  $\sim 6pN$  per MT. We deduced that a value of  $k_{nucleus} = 20pN/\mu\text{m}$  matches the elasticity of the nucleus observed in living cells.

## Microtubule Dynamics

### Free Growth Velocity

Experimental values for the average growth velocity  $v_0$  of free MTs in *S. pombe* (i.e. in the cytoplasm without opposing force) range from  $0.032$  to  $0.06\mu\text{m}/s$  (6, 14, 21). For the reference set of parameters we used a medial value  $v_g = 0.04\mu\text{m}/s$ . Because  $v_0$  has a strong influence on all traits, it was varied in our study (see main article).

### Shrinkage Velocity

Measured values for the shrinkage velocity  $v_s$  of MTs in *S. pombe* range from  $0.07\mu\text{m}/s$  (22) to  $0.21\mu\text{m}/s$  (11). We chose a medial value of  $0.15\mu\text{m}/s$  (the shrinkage velocity is specified as a negative speed in the simulation parameter file). Since the length distribution of MTs does not depend on  $v_s$  in the absence of rescues, we do not expect this parameter to influence the traits (data not shown).

### Free Catastrophe Rate

The free catastrophe rate  $c_0$  defines the probability of catastrophe for MTs which are not influenced by position or force, i.e. MTs which grow unhindered in the cytoplasm. *In vivo* measurements of  $c_0$  are complicated for the following reasons: Firstly, only catastrophes of the longest MTs within a bundle can easily be registered, since shorter MTs are difficult to detect by light microscopy. Secondly the rates measured this way usually include catastrophes that occurred at the cell poles (6, 23) presumably under the influence of forces. An upper bound for the free catastrophe rate can be obtained theoretically from the requirement that 90% of all MT bundles reach the cell poles (not shown).

### Rescue Rate

There is no report that shrinking MTs in *S.pombe* ever rescue within the cytoplasm. Accordingly the cytoplasmic rescue rate is set to zero in the simulation.

## Microtubule Response to Force

MT behavior under force is influenced by three parameters: The flexural rigidity  $\kappa_{mt}$  which defines bending, the sensitivity to force  $f_s$ , which affects the assembly rate and  $c_{stalled}$ , which controls the increase of the catastrophe rate.

### Flexural Rigidity of Microtubules

The flexural rigidity of MTs  $\kappa_{mt}$  determines how MTs bend under compressive forces. *In vitro* measurements range from  $5pN\mu m^2$  (24) up to  $40pN\mu m^2$  (7). We used  $\kappa_{mt} = 30pN\mu m^2$ . The effective bending elasticity of MT bundles can be higher than just the sum of their individual MTs, if the MTs cannot slide relative to each other longitudinally. This does not seem to be the case in *S. pombe* however, since MTs sometimes bend away from the rest of the bundle. Accordingly, in the simulation (parallel) MTs are not connected outside of the region of overlap.

### Sensitivity to Force

The parameter  $f_s$  defines the exponential dependence of the growth velocity  $v_g$  on force (see eq. 2). The value used in the simulation was measured using pure tubulin (7). In these experiments the normalized force  $f/\kappa_{mt}$  was determined from the shape of MTs, assuming they behave like homogeneous elastic rods (25). Plotting the growth velocity  $v_g$  against  $f/\kappa_{mt}$  uncovered an exponential relationship, which was fitted using 3 parameters  $A, B$  and  $C$  to  $v_g = A \exp(C f/\kappa_{mt}) - B$ . Combining the published value of  $C = 18 \pm 4\mu m^2$  (7), with our chosen flexural rigidity  $\kappa_{mt} = 30pN\mu m^2$  provided  $f_s = \kappa_{mt}/C = 1.67pN$ . One should not necessarily expect that MT *in vivo* have the same sensitivity than *in vitro*. The fact that a simulation based on these values match the *in vivo* traits is a remarkable result of our study.

### Catastrophe Rate for Stalled Microtubules

*In vitro*, rapidly growing MTs have a higher lifetime (8), following a simple linear relationship (see part B). If MT growth is stalled completely by an opposing force ( $v_g = 0$ ), catastrophe is observed within 24s on average. This value was shown to be independent of tubulin concentration (8), which suggests that it can be applied for *S. pombe* even if the tubulin concentration is unknown. We thus used the measured value  $c_{stalled} = 0.04/s$ .

## Microtubule Bundles

### Number of Bundles

Wild type cells contain between 3 and 5 MT bundles (6, 14, 11), and we have used  $N_{bundle} = 4$ .

### Bundle Structure

The structure of simulated MT bundles is specified by the number of MTs per bundle  $N_{mt}$  and the width of the overlap zone  $l_{overlap}$  (Fig. S2). Experimentally, the number of MTs per bundle was first determined from images of cells labeled with GFP-tubulin. From the stepwise increase in fluorescence intensity it was estimated that  $N_{mt} = 2$  or 3 (6). Electron tomography revealed that the bundle associated to the Spindle Pole Body (SPB) contains more MTs ( $5.7 \pm 1.5$ ) than the remaining ones ( $3.25 \pm 2.5$ ) (12). For simplicity, all bundles in the simulation were constructed equally using  $N_{mt} = 4$  (2 MTs facing each side).

The width of the overlap can be determined by imaging cells labeled with GFP-tubulin. Analyzing again the stepwise increase in the fluorescence signal results in an overlap length of  $0.84 \pm 0.29 \mu m$  (6). More direct measurements of the antiparallel bundling protein ase1p-GFP give  $1.4 \pm 0.5 \mu m$  (11). We chose a medial value of  $l_{overlap} = 1 \mu m$ .

In wild type cells, separation of MT bundles is rare (0.06/min) (15), allowing us to neglect such events in the simulation. On the contrary, bundles do not fall apart under their own polymerization force even when they push at both cell poles. In the simulation, strong links ( $k_{bundle} = 1000 pN/\mu m$ ) were used to simulate the bundling proteins, e.g. ase1p, which is thought to crosslink antiparallel MTs (11). Higher values of  $k_{bundle}$  gave identical results (data not shown).

## Numerical Parameters

Several parameters are specific to the numerical solver and to the discretization of MTs, and should not influence the outcome of the simulation. Lower values for these parameters lead to more accurate results but also require a higher number of calculations and therefore slow down the simulation. To choose an appropriate set of values we looked at the behavior of the simulation upon modifications of these parameters (Fig. S7). These tests guaranteed that the errors associated with the numerical calculations were low enough for the purpose of our study.

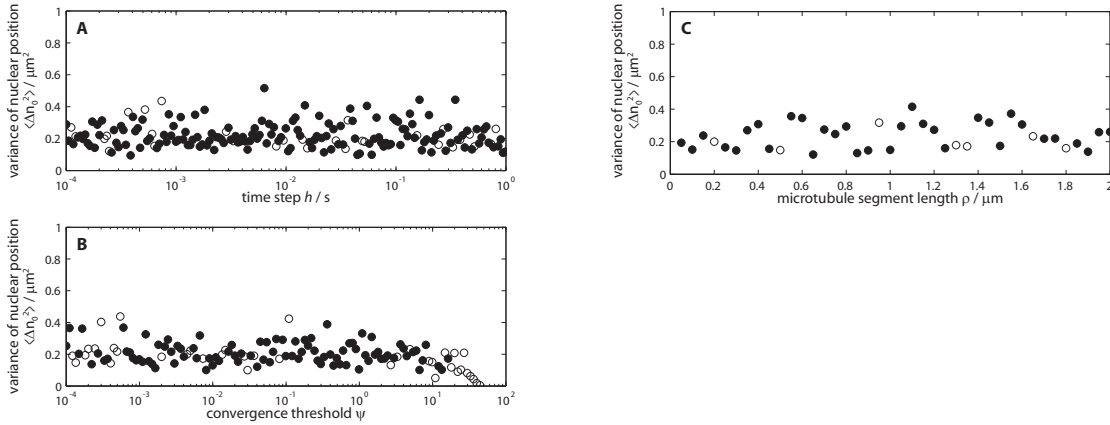


Figure S7: Variation of numerical parameters. The variance of the nuclear position  $\langle \Delta n_0^2 \rangle$  is shown as a function of the integration time-step  $\tau$  (A), the convergence  $\psi$  (B) and the segment length  $\rho$  (C). Symbols are filled if the nucleus was centered within 30 min, and open otherwise. The variability is normal and due to the stochastic nature of the simulation. A higher time step could be used, as well as a longer segment length. A convergence of  $\psi = 0.1$  was used in this study, and the results of the simulation are consistent for  $\psi < 10$ .

## E: Methods for figure 3D-E

We quantified microtubule (MT) curling in *Schizosaccharomyces pombe* by measuring the angles of the MT tips with the cell axis at the time of catastrophe. We also measured cell width and length in order to produce figures 3D-E.

### Simulations (Figure 3D)

500 simulations were performed, randomly varying cell shape: cell length was varied between 7.5 and 18  $\mu m$ , and cell diameter between 2.5 and 6  $\mu m$ . The nucleus size was scaled with the cell width, such that  $r_{nucleus}/r_{cell} = 0.75$ . The other parameters were set as in table S1. For each catastrophe event affecting the longest MT in a half-bundle, the MT direction at the plus-end is recorded in a file.

### Experimental Quantification (Figure 3E)

The objective of the experiment is to extract the position and orientation of MT tips at the moment just before they undergo a catastrophe. The following wild-type and *tea1* $\Delta$  strains were used:

1. DB 1197: h- *lys1+::nmt1-GFP- $\alpha 2$  tub ura4-D18* (integrated GFP- $\alpha 2$ -tubulin along with endogenous  $\alpha 2$ -tubulin present);
2. DB 1878: *lys1+::nmt1-GFP- $\alpha 2$  tub tea1 $\Delta$ ::ura4+ ura4-D18*.

Cells were grown on EMM2+ *ade+ his+ leu+ ura+ Th* plates at 25°C. Preculture and culture were done in EMM2 + *his + leu+ ura+ Th* for DB 1878 and in EMM2+ *ura+ Th* for DB 1197 at 25°C. Concentration of Thiamine (Th) was 15  $\mu M$ . Two hours before imaging cells were put to 36°C. Imaging was done on lectin-covered MatTek Corp. glass bottom culture dishes at 36°C. Stacks of images that covered the entire cell were acquired every 3 seconds (some movies were taken with 4s intervals), with 0.2  $\mu m$  Z-spacing on PerkinElmer Ultraview ERS spinning disk microscope.

Analysis was done using custom software developed in Matlab (R2007a), using ImageJ for file-format conversions. Detection of catastrophe time was done manually by looking for discernible shrinkage from the maximum projections movies. For each detected catastrophe, the bundle position in 3D was extracted semi-automatically in the frame just prior to catastrophe. Two mouse clicks were performed: the first one at the very tip of the bundle, and the second one on the bundle. The rest of the tracking was done automatically by marching along the maximum intensity in 3D from the initial user click. The next point of the bundle in XY plane is defined from the maximum of intensity on an arc of a circle centered on the previous point. The arc covers 180° such that the detection of the bundle progresses in one direction. The diameter of this circle is 5 pixels, which corresponds to the apparent diameter of MTs. The position in Z of the bundle tip was defined by finding the Z-value with maximal intensity. The search for the subsequent points was limited to the adjacent Z-planes to the Z-position of the previous point (3 planes in total). In this way, a 3D representation of the MT near the MT tip is obtained. It is then smoothed using smoothing spline function (Matlab), in order to define more precisely the tangent vector at the end of the bundle.

The geometric parameters of the cell (length and width) are extracted from brightfield image taken at the Z-position of maximal contrast. From this view, the coordinate system is also adjusted to place the origin at the cell tip closest to the point of catastrophe, with the X axis oriented along the cell axis towards the cell center. The Z axis is unchanged and the Y axis is set to create an ortho-normal reference.



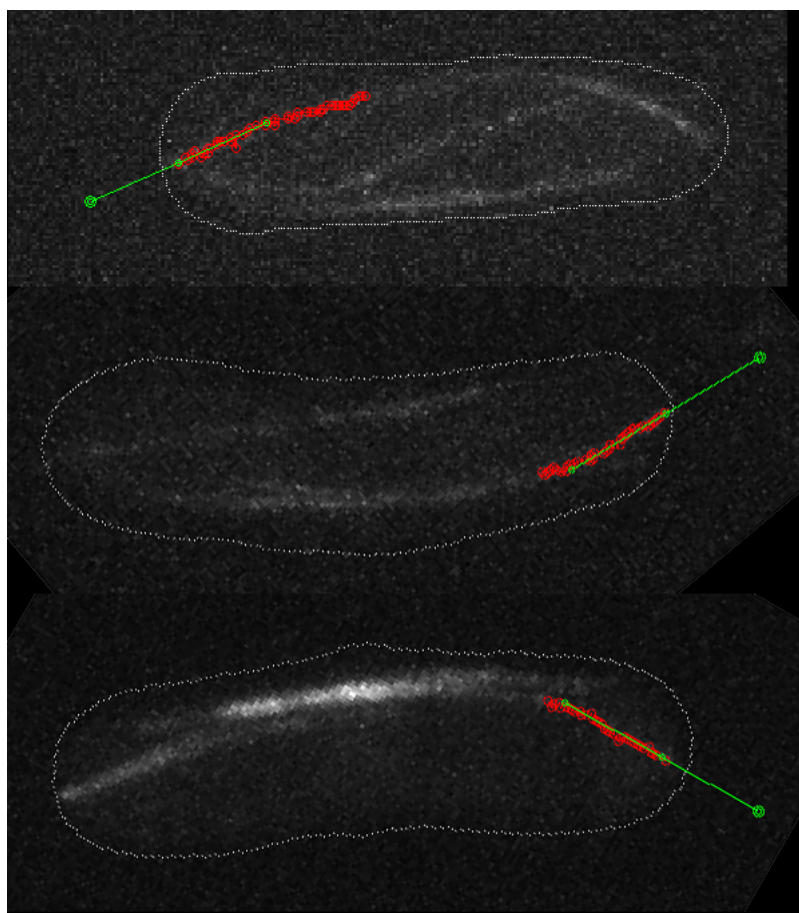


Figure S8: Examples of extracted microtubule directions just prior of catastrophe.

## References and Notes

1. E. M. Purcell, *Am J Phys* **45**, 3 (1977).
2. F. Nedelec, D. Foethke, *New Journal of Physics* **9**, 427 (2007).
3. H. C. Berg, *Random Walks in Biology* (Princeton University Press, 1993).
4. P. M. Bungay, H. Brenner, *Int J Multiphase Flow* **1**, 25 (1973).
5. R. R. Daga, A. Yonetani, F. Chang, *Curr Biol* **16**, 1544 (2006).
6. P. T. Tran, L. Marsh, V. Doye, S. Inoué, F. Chang, *J Cell Biol* **153**, 397 (2001).
7. M. Dogterom, B. Yurke, *Science* **278**, 856 (1997).
8. M. E. Janson, M. E. d. Dood, M. Dogterom, *J Cell Biol* **161**, 1029 (2003).
9. D. Brunner, P. Nurse, *Cell* **102**, 695 (2000).
10. A. Yamamoto, R. R. West, J. R. McIntosh, Y. Hiraoka, *J Cell Biol* **145**, 1233 (1999).
11. I. Loïdouce, *et al.*, *Mol Biol Cell* **16**, 1756 (2005).
12. J. L. Höög, *et al.*, *Dev Cell* **12**, 349 (2007).
13. R. Behrens, P. Nurse, *J Cell Biol* **157**, 783 (2002).
14. M. E. Janson, T. G. Setty, A. Paoletti, P. T. Tran, *J Cell Biol* **169**, 297 (2005).
15. R. E. Carazo-Salas, P. Nurse, *Nat Cell Biol* **8**, 1102 (2006).
16. I. M. Tolić-Nørrelykke, E.-L. Munteanu, G. Thon, L. Oddershede, K. Berg-Sørensen, *Phys Rev Lett* **93**, 78102 (2004).
17. F. R. Neumann, P. Nurse, *J Cell Biol* **179**, 593 (2007).
18. L. Zheng, C. Schwartz, L. Wee, S. Oliferenko, *Mol Biol Cell* **17**, 2212 (2006).
19. R. Ding, R. R. West, D. M. Morphew, B. R. Oakley, J. R. McIntosh, *Mol Biol Cell* **8**, 1461 (1997).
20. P. G. Saffman, M. Delbrück, *Proc Natl Acad Sci U S A* **72**, 3111 (1975).
21. K. E. Busch, J. Hayles, P. Nurse, D. Brunner, *Dev Cell* **6**, 831 (2004).
22. D. R. Drummond, R. A. Cross, *Curr Biol* **10**, 766 (2000).
23. K. E. Busch, D. Brunner, *Curr Biol* **14**, 548 (2004).
24. F. Gittes, B. Mickey, J. Nettleton, J. Howard, *J Cell Biol* **120**, 923 (1993).
25. L. D. Landau, E. M. Lifshitz, *Theory of Elasticity* (Pergamon Press, 1986).